Eur. Phys. J. B **38**, 111–115 (2004)
DOI: 10.1140/epjb/e2004-00106-1

THE EUROPEAN PHYSICAL JOURNAL B

$\sqrt{3}$ linear structures in the Te/Ni(111) system

S. Suehara[a], T. Aizawa, S. Hishita, A. Nukui, and S. Inoue

Advanced Materials Laboratory, National Institute for Materials Science, 1-1 Namiki, Tsukuba, Ibaraki 305-0044, Japan

Received 14 April 2003 / Received in final form 1st December 2003
Published online 20 April 2004 –

Abstract. Surface structures in the Te/Ni(111) system are revealed by using reflection high-energy electron diffraction combined with X-ray and ultraviolet photoelectron spectroscopies. At a 0.33 mono-layer (ML)-Te/Ni(111) surface, a reversible structural phase transition is observed with a transition temperature T_c of 380 °C. The diffraction pattern from the low temperature phase is accompanied by streaks. The high and low temperature phases are characterized by $\sqrt{3}\times\sqrt{3}R\pm30°$ and $3\times\sqrt{3}$ rectangle, respectively. The mechanism of the phase transition is explained by the order-disorder transition with a rumpled chain model. Both 0.51 ML- and 0.44 ML-Te/Ni(111) surfaces exhibit the complex diffraction patterns accompanied by diffuse streaks. These surface structures are characterized by the $7\times\sqrt{3}$ rectangle and $5\sqrt{3}\times\sqrt{3}R\pm30°$, respectively. All diffuse streaks obtained at the above surfaces are consistently interpreted in the view of the *ill*-ordered arrangements of the *well*-ordered $\sqrt{3}$ linear chains. It is shown that the "$\sqrt{3}$ linear structure" is the key in the Te/Ni(111) system.

PACS. 61.14.Hg Low-energy electron diffraction (LEED) and reflection high-energy electron diffraction (RHEED) – 68.65.-k Low-dimensional, mesoscopic, and nanoscale systems: structure and nonelectronic properties – 64.60.Cn Order-disorder transformations; statistical mechanics of model systems

1 Introduction

Adsorbate-induced relaxation and reconstruction of metal surfaces have been the subjects of numerous investigations over the last few decades. In particular, the adsorption of sulfur on nickel metal surfaces has been intensively studied in terms of catalytic properties, and many complex surface reconstructions have been found [1–5]. At S/Ni(111) surfaces, for example, $\sqrt{39}$-S for 0.22 monolayer (ML), $p(2\times2)$-S for 0.25 ML, $(\sqrt{3}\times\sqrt{3})R30°$-S for 0.33–0.48 ML, $(5\sqrt{3}\times2)$-S for 0.4 ML, and (8×2)-S for 0.44 ML have been reported [6–8]. On the other hand, the Te/Ni(111) system is not researched as long as we know. Because a Te atom belongs to the same 16-group (chalcogen) as an S atom, various surface structures are expected on this system. Te surface layers on other substrates have recently attracted considerable attention in both fundamental and technological research fields [9–14].

In this paper we present the surface structures of the Te/Ni(111) system studied by reflection high-energy electron diffraction (RHEED). The overlayer coverage and the electronic state were measured by X-ray photoelectron spectroscopy (XPS) and ultraviolet photoelectron spectroscopy (UPS). The absolute coverage was calibrated by using Rutherford backscattering spectroscopy (RBS) combined with a computer simulation. The four different structures are found according to the Te coverage and the substrate temperature. The key of these surface structures is discussed and suggested to be a "$\sqrt{3}$ linear structure" as a base structure of this system.

2 Experimental

The apparatus used in this investigation is the accelerator linked instrument for synthesis and analysis (ALISA) in our institute. ALISA consists of a Van-de-Graaf-type accelerator(200–2000 kV) and several interconnected vacuum chambers. A deposition chamber, in which the Te deposition and the in situ RHEED observation were performed, is equipped with an electron gun (VG scientific, LEG-110), a quartz thickness monitor, and a Knudsen cell (K-cell) with a BN crucible. The chamber is evacuated by a 400 l/s turbo-molecular pump and achieved an ultra-high vacuum (UHV) in the pressure range of 10^{-8} Pa. The XPS and UPS experiments were done in another chamber (VG scientific, ESCALAB-200X), which is equipped with a twin-anode X-ray source, a hemispherical analyzer, and a multipurpose ion gun (VG scientific, EX05) for sputter cleaning and/or etching. The RBS measurement was performed in another chamber. A sample transfer system connects these chambers and enables the sample to move between them in a UHV. The electron beam of 10–15 kV was employed for RHEED. 2000 keV-He^+ ions were utilized for

[a] e-mail: suehara.shigeru@nims.go.jp

the RBS measurement. XPS spectra were recorded using an Mg $K\alpha$ ($h\nu$ =1253.6 eV) source with an instrument resolution of less than 1.0 eV. The accuracy of UPS work function measurements with HeII ($h\nu$ = 40.8 eV) source was estimated to less than ±20 meV.

A sample exposing a (111) surface was cut by spark erosion from a nickel single crystal rod grown by the floating zone method. The sample was mechanically polished to a mirror finish with alumina powder, and then electrochemically polished in a solution of HNO_3 (33 vol.%) and C_2H_5OH (67 vol.%). The sample was held on Ta wires and can be heated in a vacuum by an electron bombardment from the backside. Sample temperatures were monitored by the TR-630A (MINOLTA Corp.) and IR-AP2CP (CHINO Corp.) optical pyrometers with an emissivity parameter ε of 0.25. The clean surface was obtained by cycles of in situ Ar^+ sputtering (typically, 3 keV, 0.2 μA, 30 min) and annealing at 1100–1200 °C. The cleaning process was repeated until no trace of sulfur, which is the last remaining impurity, was recognized in the AES spectrum. The clean surface displayed a sharp 1×1 RHEED pattern.

High-purity (99.9999%) Te was evaporated by the K-cell, which was automatically temperature-controlled in the range of 220–300 °C, onto the room temperature (RT) substrate of the Ni(111) 1×1 surface at a rate of ∼0.5 ML/min (1 ML: monolayer = 1.86×10^{19} m^{-2}). The evaporation rate was monitored with the quartz-crystal microbalance (Te coverage was estimated from the bulk density of Te (6.24 g/cm^3)). After ∼1 ML-Te deposition, we performed the sample heating and cooling at typical rates of ∼5 °C/min and ∼1 °C/min, respectively, under in situ RHEED observation. Interesting structures were the object of the XPS and UPS measurements.

3 Results

After ∼1 ML-Te adsorption, the RHEED shows no clear diffraction pattern indicating the amorphousness of the overlayer. The sample was gradually heated during the RHEED observation. When the temperature reached to ∼250 °C, the RHEED pattern changed to show streaks. Figures 1a and 1b show the RHEED patterns obtained by cooling the substrate to RT just after the appearance of streaks. Taking into account the rotational symmetry of the substrate, this surface is interpreted as a three-domains structure as shown in Figure 1c. As the reciprocal lattice is streaky along the $\langle 1\bar{1}0\rangle$ directions, the $\frac{1}{3}$-order reflections are observed although there is no spot in the reciprocal space. Figure 1e shows the real lattice derived from the reciprocal lattice for a domain (Fig. 1d). The surface unit cell is characterized by the $7 \times \sqrt{3}$ rectangle as shown in Figure 1e, which is described as, for example, $\begin{vmatrix} 1 & -1 \\ 7 & 7 \end{vmatrix}$ by the matrix notation. This surface structure is not describable in Wood's notation [15] since it is rectangular on a hexagonal substrate. In the following, however, we use a simplified Wood's notation like "$7 \times \sqrt{3}$" even in such cases for convenience sake.

A similar but different RHEED patterns shown in Figures 1f and 1g were obtained after prolonged annealing at ∼300 °C for 10 min. The difference is $\frac{1}{15}$-order reflection spots in place of the $\frac{1}{14}$-order reflections in Figure 1a. Figures 1h–j show the deduced reciprocal lattice and the periodicity in the real space. The reciprocal lattice is streaky along the $\langle 1\bar{1}0\rangle$ directions also in this case. This surface is characterized by $5\sqrt{3} \times \sqrt{3}R \pm 30°$ three-domains structure (which is described as, for example, $\begin{vmatrix} 1 & -1 \\ 10 & -5 \end{vmatrix}$ by the matrix notation) as shown in Figure 1j.

The streaky RHEED pattern changed into a halo pattern over 580 °C. During cooling the sample from ∼700 °C, two kinds of RHEED patterns were observed. One was a $\sqrt{3} \times \sqrt{3}R \pm 30°$ structure, which was observed at higher temperature than 380 °C. The other was a $2\sqrt{3} \times 2\sqrt{3}R \pm 30°$ structure (Figs. 1k and 1l) at lower temperature than 380 °C. These two surface structures were confirmed to have a reversible phase transition at the temperature T_c of 380 °C. In the low temperature phase, two periodicities in the real space can give the same RHEED pattern. Figures 1m–q show the schematic illustrations of the diffraction pattern and the possible real lattices derived from it. Interpretation by a single-domain model (Fig. 1n) leads the $2\sqrt{3} \times 2\sqrt{3}R \pm 30°$ structure, and by a three-domains model, the $3 \times \sqrt{3}$ rectangular structure (which is identical to $2\sqrt{3} \times \sqrt{3}R \pm 30°$ structure. See Fig. 1q) is derived. In Figure 1k, the interval between the reflections in the $\frac{1}{2}$th Laue zone is twice of that in the 0th Laue zone. Only the right-going streaks appear there. This is not explained by the single-domain model but is well explained by the three-domains model with the unbalanced domain growth. Thus, this low temperature phase is concluded to have the $3 \times \sqrt{3}$ rectangular three-domains structure (which is described as, for example, $\begin{vmatrix} 1 & -1 \\ 3 & 3 \end{vmatrix}$ by the matrix notation) rather than the $2\sqrt{3}\times2\sqrt{3}R\pm30°$ single-domain one. It must be noted that the RHEED patterns are accompanied by similar streaks found in the $7 \times \sqrt{3}$ or $5\sqrt{3} \times \sqrt{3}$ structure.

XPS and UPS spectra were measured for the three structures found: $7 \times \sqrt{3}$, $5\sqrt{3} \times \sqrt{3}$, and $3 \times \sqrt{3}$ structures. In order to determine the absolute coverage of Te, RBS measurement for the $3\times\sqrt{3}$ structure was performed. By comparing the spectrum with the RUMP computer simulation [16], the coverage was estimated to 0.33 ML (0.62×10^{19} m^{-2}). Taking this surface as a standard, the Te coverages were estimated from the Te $3d_{5/2}$ XPS peak intensity ratios (Ni LMM peaks found in the region of 403–541 eV were utilized for normalizing the intensity of each spectrum). Table 1 summarizes Te coverages (θ), work functions (ϕ), and Te $3d_{5/2}$ binding energies ($E_{\mathrm{Te}3d_{5/2}}$) of the Te/Ni(111) surfaces with those of clean Ni(111), Te (bulk) and tellurides for comparisons. ϕ were estimated from the differences between the HeII energy and the widths of the UPS spectra determined by the cutoff and Fermi edges.

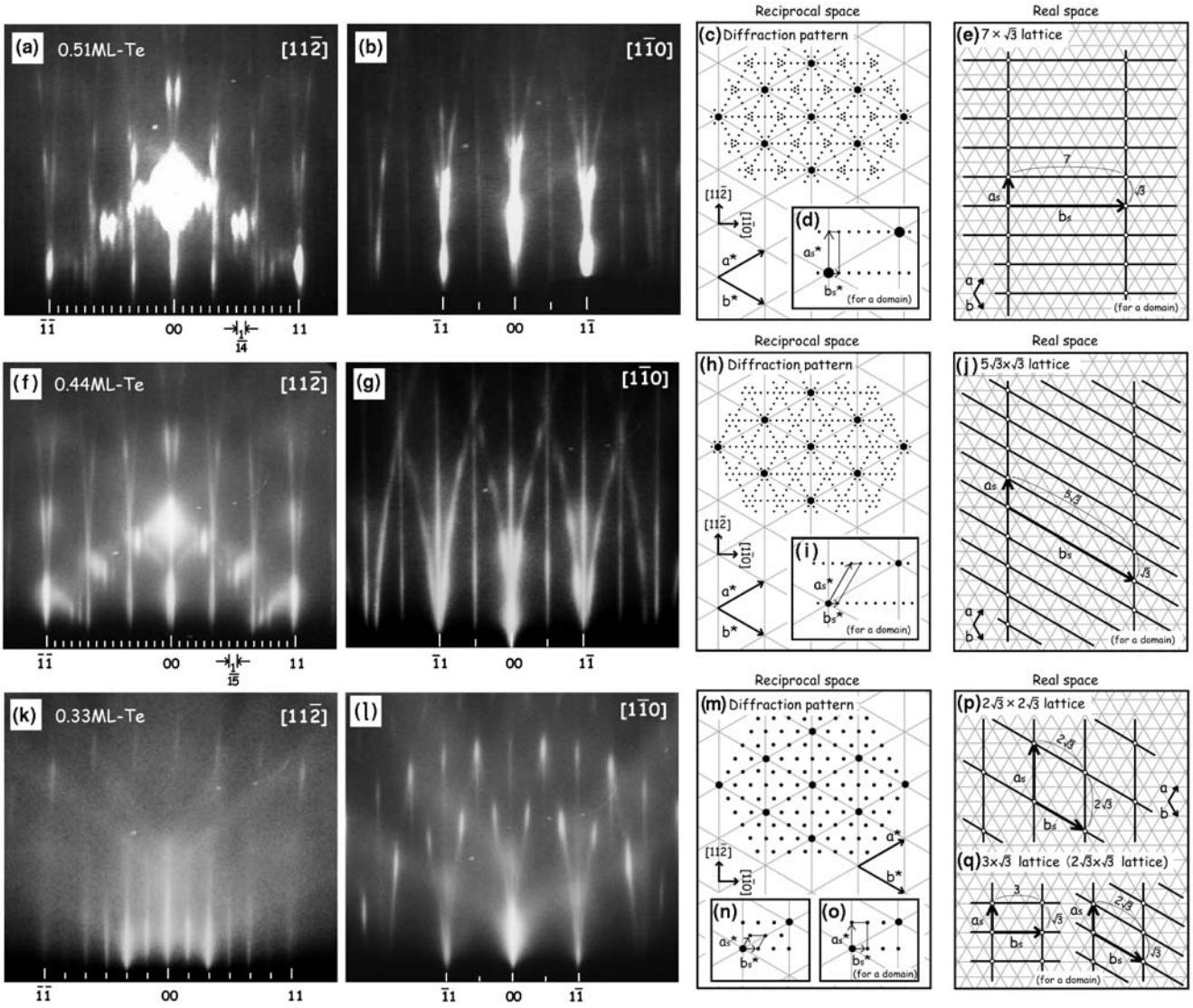

Fig. 1. RHEED patterns of 0.51 ML-, 0.44 ML-, and 0.33 ML-Te/Ni(111) surfaces observed in $\langle 11\bar{2}\rangle$ and $\langle 1\bar{1}0\rangle$ azimuths and schematic illustrations of them as in reciprocal and real spaces. Primitive vectors are defined by a and b for a substrate unit cell, and a_s and b_s for a surface unit cell. Asterisk (*) denotes corresponding reciprocal vectors.

The adsorption of Te on the Ni(111) substrate decreased the work function from 5.5 eV to ∼4.7 eV. $E_{\mathrm{Te}3d_{5/2}}$, which were determined by applying the conventional curve fitting technique using Voigt function to the respective XPS peak spectrum from which the nonlinear background was subtracted [17], of the Te/Ni(111) surfaces were within the range of those of tellurides.

Table 1. Measured Te coverages (θ), work functions (ϕ), and Te $3d_{5/2}$ XPS binding energies ($E_{\mathrm{Te}3d_{5/2}}$) with full widths at half maximum in the parentheses.

Surface	θ (ML)	ϕ (eV)	$E_{\mathrm{Te}3d_{5/2}}$ (eV)
Ni(111)$7\times\sqrt{3}$-Te	0.51	4.7	572.7(1.8)
Ni(111)$5\sqrt{3}\times\sqrt{3}$-Te	0.44	4.7	572.7(1.7)
Ni(111)$3\times\sqrt{3}$-Te	0.33	4.6	572.6(1.5)
Ni(111)		5.5	
Te(bulk)		4.8 [18]	572.9 [19]
Tellurides			572.3–572.7 [19]

4 Discussion

The 0.33 ML adsorption corresponds to one adsorbed atom per a $\sqrt{3}\times\sqrt{3}$ unit cell. Determining the adsorption site is the remaining problem. Chemical modifications of tellurium appear to be similar to those of sulfur. On the analogy of the Ni(111)$\sqrt{3}\times\sqrt{3}R30°$-S surface [8], it could be suggested that a Te atom adsorbs on a hollow site in the high temperature $\sqrt{3}\times\sqrt{3}$ phase. However, it changes to the stabler $3\times\sqrt{3}$ structure below T_c (380 °C), which was not found in the S/Ni(111) surface. From the electron negativities of Te and Ni atoms (2.1 and 1.8, respectively [20]) and the Te $3d_{5/2}$ binding energies shown

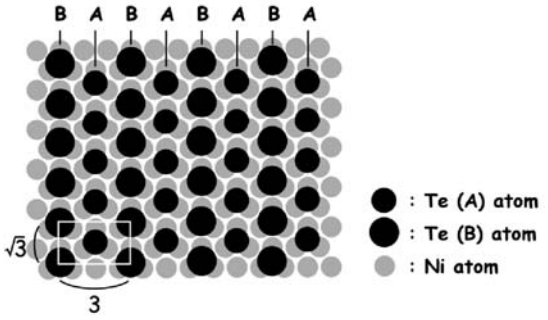

Fig. 2. A rumpled chain model for a domain of the $3 \times \sqrt{3}$ low temperature phase. All Te atoms occupy the three-fold hollow sites of Ni(111) at the two adsorption heights, lower (A) and higher (B). Te(A) and Te(B) make $\sqrt{3}$ linear chains A and B, respectively.

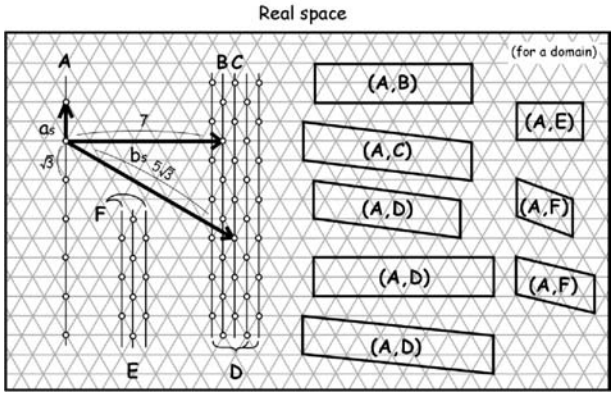

Fig. 3. Schematic illustration of the Te/Ni(111) surfaces in real space. a_s and b_s are primitive surface vectors. A, B, C, D, E, and F represent $\sqrt{3}$ chains. A combination of chain A with one of the other chains defines a surface structure. For example, the combination of chain A with chain B offers a surface unit cell (A, B) (i.e. the $7 \times \sqrt{3}$ phase).

in Table 1, the surface Te atoms on Ni(111) should be in a negative charged state. Since the Te ionic diameter in tellurides (0.442 nm [20]) is larger than the distance between the identical sites in the $\sqrt{3} \times \sqrt{3}$ structure at the Ni(111) surface (0.431 nm), it is most likely that the surface Te atoms form a rumpled layer where some atoms are moved up vertically to the surface. The $\sqrt{3} \times \sqrt{3}$ structure at high temperature phase can be explained by the disordered phase of this rumpled layer: a Te atom at this surface is moving, vibrating around a hollow site, losing the order in the rumpling structure. This disordered phase has the average structure of $\sqrt{3} \times \sqrt{3}$. The phase transition at T_c is interpreted as the order-disorder transition.

We propose a rumpled chain model for the $3 \times \sqrt{3}$ structure as shown in Figure 2. In this model, all Te atoms occupy the three-fold hollow sites of Ni(111) at the two adsorption heights, lower (A) and higher (B). These Te atoms make $\sqrt{3}$ linear chains A and B, respectively (Fig. 2). If the rumpling occurs by the repulsive force between the chains, it is reasonable to consider a vacant chain at the site B. The vacant chain may release the compressive stress in the vicinity, which can cause weak rumpling or longer periodicity around it. Additionally, the registry of the chains can be altered at this site to make a phase boundary. In this model, the coherent length across the chain is small because of the phase boundaries and the possible fluctuation of the periodicity near them. The streaky RHEED pattern is well explained by the small region size across the chain.

Since a 0.33 ML-Te completely covers up the Ni(111) surface as discussed above, surface Te atoms should consist of, at least, two layers at both the $5\sqrt{3} \times \sqrt{3}$ (0.44 ML-Te) and $7 \times \sqrt{3}$ (0.51 ML-Te) phases. Charge states of Te atoms at the second layer must be closer to neutral than that at the first layer, because Te atoms at the second layer contact with only Te atoms. This is suggested by the Te $3d_{5/2}$ binding energy and the work function approaching to the respective values of Te (bulk) as the Te coverage increases as shown in Table 1 although the amounts of these shifts are small. It is difficult to propose a reasonable structure model within a simple ionic/atomic diameter view for these phases because in these surfaces, at least, two kinds of Te (the first layer Te atoms strongly affected by the Ni(111) surface potential, and the second one which is less charged and surrounded by only Te atoms) exist.

Generally, diffuse streaks on diffraction patterns often come from a not-well-ordered surface which should be traced to an inadequate thermal treatment. The 0.51 ML-Te/Ni(111) surface may be attributed to this case since this surface isn't annealed and shows larger FWHM of the Te $3d_{5/2}$ peak than the other surfaces (Tab. 1). However, the annealed surfaces, i.e. 0.44 ML-Te/Ni(111) and 0.33 ML-Te/Ni(111) also give the diffraction patterns accompanied by diffuse streaks. This fact suggests that these surfaces have some intrinsic structures profoundly associated with the disorder. A diffuse streak reflection appears from lack of the long-range ordering along the corresponding direction. Therefore, the streaks found in the RHEED patterns indicate the coexistence of both *ill* and *well* orderings along the b_s and a_s surface vectors, respectively. Figure 3 shows the schematic illustration of these surfaces. Here, let us consider on two adjacent identical chains A and B consisting of the $\sqrt{3}$-spaced lattice points along an a_s surface vector on the surface. These chains are elements to give $\sqrt{3}$ reflections and the combination of chains A and B defines a surface unit cell as indicated by (A, B) in Figure 3 (i.e. the $7 \times \sqrt{3}$ rectangle). Thus, each combination of the chain A with one of the nearest identical chains determines the respective surface unit cell. The streak is originated from the small coherent region in the direction across the chain. Since the features of the surface unit cells given by (A, B), (A, C), and (A, D) seem to be little different from each other as seen in Figure 3, it is most likely that the (A, B), (A, C), (A, D), and the other similar structures can coexist naturally at around 0.44–0.51 ML coverage of Te. If some amount of (A, C) and/or (A, D) parts exists in major (A, B) lattices in the $7 \times \sqrt{3}$ surface, they play anti-phase boundaries which reduces the coherent length. The same is true in the $5\sqrt{3} \times \sqrt{3}$ and $3 \times \sqrt{3}$ surfaces. The possible registry change at the boundary is

shown in Figure 3 as (A, E) and (A, F). Thus, the diffuse streaks obtained at all presented surfaces (0.33 ML-, 0.44 ML-, and 0.51 ML-Te/Ni(111)) can be explained by the surface unit cells determined by *ill*-ordered arrangements of the *well*-ordered $\sqrt{3}$ linear chains. It means that the "$\sqrt{3}$ linear structure" is the key in the Te/Ni(111) system.

5 Summary

We have presented surface structures of the Te/Ni(111) system with use of RHEED, XPS, and UPS. The 0.33 ML-Te/Ni(111) surface exhibited the reversible structural phase transition with the transition temperature of 380 °C. The high and low temperature phases were characterized by $\sqrt{3} \times \sqrt{3}R \pm 30°$ and $3 \times \sqrt{3}$ rectangle, respectively. We proposed the order-disorder transition of the rumpled $\sqrt{3}$ linear chains. The 0.51 ML- and 0.44 ML-Te/Ni(111) surfaces were characterized by $7 \times \sqrt{3}$ rectangle and $5\sqrt{3} \times \sqrt{3}R \pm 30°$, respectively. The diffuse streaks obtained at all presented surface were consistently interpreted in the view of the *ill*-ordered arrangements of the *well*-ordered $\sqrt{3}$ linear chains. It was shown that the "$\sqrt{3}$ linear structure" is common in the Te/Ni(111) structures.

References

1. P. Delescluse, A. Masson, Surf. Sci. **100**, 423 (1980)
2. T. Edmonds, J.J. McCarroll, R.C. Pitkethly, J. Vac. Sci. Technol. **8**, 68 (1971)
3. L. Ruan, I. Stensgaard, F. Besenbacher, E. Laegsgaard, Phys. Rev. Lett. **71**, 2963 (1993)
4. M. Foss, R. Feidenhans'l, M. Nielsen, E. Findeisen, R.L. Johnson, T. Buslaps, I. Stensgaard, F. Besenbacher, Phys. Rev. B **50**, 8950 (1994)
5. G. Koller, F.P. Netzer, M.G. Ramsey, Surf. Sci. **421**, 353 (1999)
6. V. Maurice, N. Kitakatsu, M. Siegers, P. Marcus, Surf. Sci. **373**, 307 (1997)
7. S. Tsukawaki, Y. Hatano, K. Hashizume, M. Sugisaki, Surf. Sci. **457**, 63 (2000)
8. S. Takenaka, T. Yokoyama, S. Terada, M. Sakano, Y. Kitajima, T. Ohta, Surf. Sci. **372**, 300 (1997)
9. F. Wiame, G. Mathot, S. Sivananthan, S. Rujirawat, R. Caudano, R. Sporken, Appl. Surf. Sci. **142**, 475 (1999)
10. K. Tamiya, T. Ohtani, Y. Takeda, T. Urano, S. Hongo, Surf. Sci. **408**, 268 (1998)
11. S.A. Yoshikawa, J. Nogami, C.F. Quate, P. Pianetta, Surf. Sci. **321**, L183 (1994)
12. M. Stolzenberg, I. Lyuksyutov, E. Bauer, Phys. Rev. B **42**, 10714 (1990)
13. M. Stolzenberg, I. Lyuksyutov, E. Bauer, Phys. Rev. B **44**, 12593 (1991)
14. M. Stolzenberg, I. Lyuksyutov, E. Bauer, Phys. Rev. B **48**, 2675 (1993)
15. E.A. Wood, J. Appl. Phys. **35**, 1306 (1964)
16. L.R. Doolitte, Nucl. Inst. Meth. B **9**, 344 (1985)
17. D. Briggs, M.P. Seah, *Practical Surface Analysis by Auger and X-ray photoelectron Spectroscopy* (Wiley, New York, 1983)
18. L. Apker, E. Taft, J. Dickey, Phys. Rev. **74**, 1462 (1948)
19. J.F. Moulder, W.F. Stickle, P.E. Sobol, K.D. Bomben, *Handbook of X-ray Photoelectron Spectroscopy: A Reference Book of Standard Spectra for Identification of XPS Data* (Physical Electronics, Inc., Minnesota, 1995)
20. G. Burns, *Solid State Physics* (Academic Press, Inc., New York, 1985)
21. R.W.G. Wyckoff, *Crystal Structures* (Interscience, New York, 1963)